Excited-State Hydroxide Ion Transfer from a Model Xanthenol Photobase

ARTICLE *in* THE JOURNAL OF PHYSICAL CHEMISTRY B · OCTOBER 2014

Impact Factor: 3.3 · DOI: 10.1021/jp5080169 · Source: PubMed

4 AUTHORS, INCLUDING:

Yun Xie

Bowling Green State University

3 PUBLICATIONS **5** CITATIONS

SEE PROFILE

Hoi Ling Luk

19 PUBLICATIONS **134** CITATIONS

SEE PROFILE

THE JOURNAL OF PHYSICAL CHEMISTRY B

Article

pubs.acs.org/JPCB

Excited-State Hydroxide Ion Transfer from a Model Xanthenol Photobase

Yun Xie, Hoi Ling Luk, Xin Yang, and Ksenija D. Glusac*

Department of Chemistry and Center for Photochemical Sciences, Bowling Green State University, Bowling Green, Ohio 43403, United States

ABSTRACT: This article reports a study of excited-state hydroxide ion release from a model xanthenol photobase, XanOH. The driving force for the reaction was tuned using solvent mixtures with varying water/acetonitrile ratios, and the kinetics of the reaction was monitored using ultrafast pump−probe spectroscopy. The intrinsic barrier for the heterolysis was evaluated using Marcus and bond-energy bond-order (BEBO) models. The obtained value ($\Delta G_o^{\#}$ = 10.17−10.80 kcal/mol) is significantly higher than the intrinsic barriers found for the proton release from previously studied photoacids. These results were discussed in terms of the difference in structures of solvated H^+ and OH^- ions.

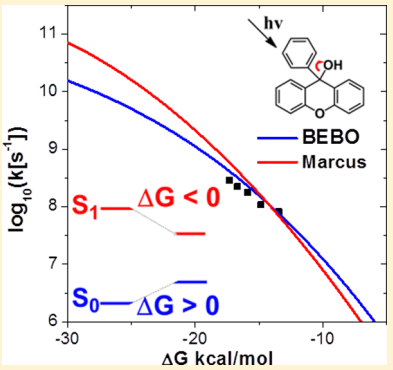

INTRODUCTION

Transmissions of H^+ and OH^- ions through aqueous media are essential processes in biology,[1] chemistry,[2] and material science.[3] The discovery of exceptionally large mobilities of H^+ and OH^- ions in water[4] has led to numerous studies of the mechanism of this fast transport, with particular focus on the proton transfer. Using combined experimental (for example, IR,[5] NMR,[6] and time-resolved vibrational pump−probe spectroscopy[7]) and computational (for example, *ab initio* molecular dynamics[8] and parametrized empirical valence bond[9]) methods, the microscopic details of the proton transfer in water has been described. A relative agreement is achieved that the proton transfer involves two steps: (i) a rate-determining hydrogen bond breakage that converts the Eigen-type 3-coordinated $H_3O^+(H_2O)_3$ cation into a centro-symmetric Zundel-type $H^+(H_2O)_2$ cation and (ii) a barrierless proton transfer from the Zundel cation. Significantly less is currently known about the hydroxide ion transfer, and the initial assumptions that the OH^- transfer is a simple "mirror image" of the H^+ transfer were recently challenged.[10] Theoretical calculations[11] and experimental neutron[12] and X-ray[13] diffraction findings suggest that the structure of OH^- in water does not resemble the expected "mirror image" $OH^-(H_2O)_3$ form but the hypercoordinated $OH^-(H_2O)_4$ structure instead. Furthermore, theoretical calculations predict that the mechanism of OH^- transfer is different from the H^+ transfer.[11] However, experimental time-resolved studies of OH^- transfer that can evaluate these theoretical predictions are still scarce.[14,15]

Photoacids are valuable probes of proton transfer kinetics in aqueous media. These compounds undergo substantial electronic redistribution upon excitation, which causes a large drop in their pK_a values.[16,17] The resulting proton release can be conveniently triggered by a laser pulse, allowing the use of ultrafast time-resolved techniques to probe details of the proton transfer mechanism. The kinetic studies using photoacids have shown that the proton transfer is mainly controlled by the solvent motion, based on the small intrinsic barrier for proton transfer (∼1.6 kcal/mol), nonlinear rate dependence on the temperature, and other effects.[18,19] A particularly interesting application of photoacids in proton transfer research is a time-resolved IR study showing the important role that water bridges play in mediating the proton transfer between the donor and the acceptor.[20] Furthermore, photoacids are often used to probe the water dynamics in confined media, such as cyclodextrins,[21] reverse micelles,[22,23] and nafion membranes.[24]

Analogous studies of hydroxide ion transfer can be performed using photobases that release OH^- ion in the excited state. Several organic structures are known to undergo excited-state hydroxide ion transfer, most of which are arylmethyl alcohols with general formula Ar_3C-OH and similar motifs.[25−33] The pseudobase pK_a values (equilibrium constants for the reaction $R-OH \rightarrow R^+ + OH^-$) of these alcohols exhibit a drastic change upon excitation: from ground-state pK_a values in the −3.7 to +0.1 range to the excited-state pK_a* values in the 22−25 range.[34] Two differences exist between photoacids and photobases: (i) unlike proton release from photoacids, the OH^- ion release from photobases is usually not adiabatic (except in the case of xanthenol where a small fraction of photogenerated cation is formed via an adiabatic route[29,30]);

Special Issue: Photoinduced Proton Transfer in Chemistry and Biology Symposium

Received: August 7, 2014
Revised: October 23, 2014
Published: October 27, 2014

dx.doi.org/10.1021/jp5080169 | J. Phys. Chem. B 2015, 119, 2498−2506

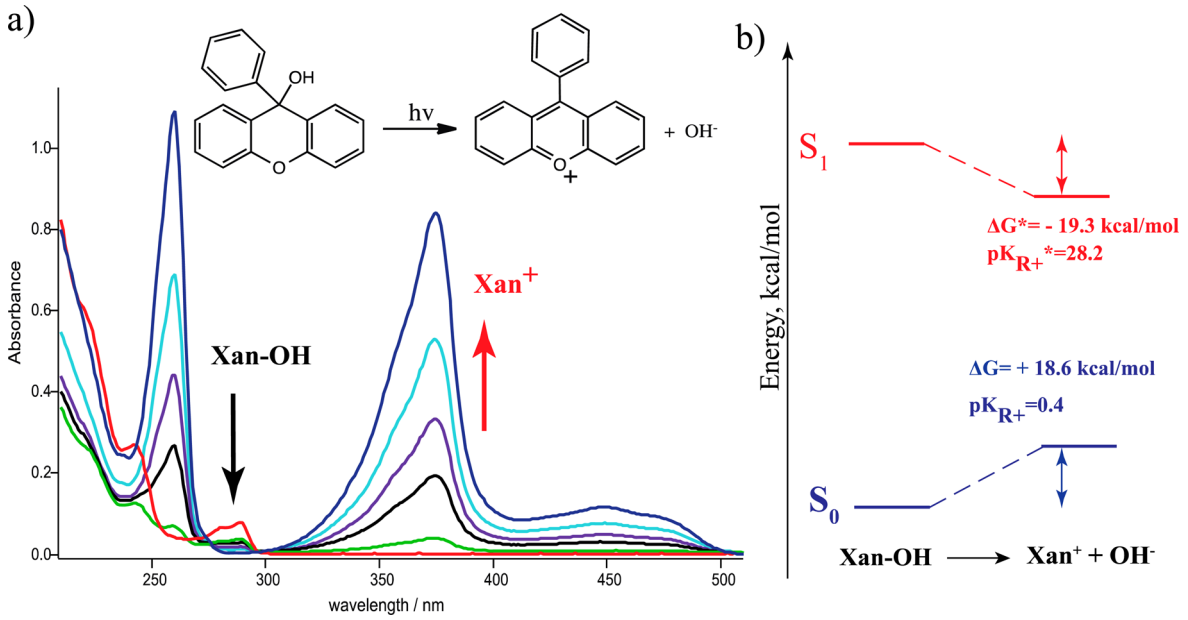

Figure 1. (a) pH-dependent conversion of aqueous XanOH to Xan^+ studied using UV/vis absorption spectroscopy (pH values: −0.46 (dark blue), 0.24 (light blue), 0.54 (purple), 0.84 (black), 1.54 (green), and 7 (red)). (b) Förster energy diagram used to evaluate the excited-state Gibbs (ΔG^*) free energy and pK_{R+}^* values for XanOH.

(ii) the photobases undergo both the heterolytic C−O bond cleavage to release OH^- ions and homolytic C−O bond cleavage to release OH• radicals, and the branching ratio between two channels can be altered by the solvent polarity.[29] In protic polar solvents, the heterolysis is favored, thus making photobases ideal systems for studies of hydroxide ion transfer processes in aqueous media. Despite this advantage, only a limited number of studies provide the insights into the mechanism of hydroxide ion transfer.[28,35]

We have previously investigated the hydroxide ion release from an acridinol-based system, and found that the process is relatively fast in protic solvents (~100 ps).[28] This work intrigued us to perform a more detailed kinetic study and evaluate the intrinsic barrier for the hydroxide ion transfer. In this work, we present a time-resolved study of excited-state hydroxide ion release from a model photobase, 9-phenyl-xanthen-9-ol (XanOH, Figure 1a). Previous steady-state and time-resolved studies have shown that, depending on the solvent, XanOH undergoes C−O bond heterolysis from the singlet excited state and/or homolysis from the triplet excited state.[29,30,36] However, the kinetics of heterolysis was not investigated in these studies due to the low temporal resolution of the flash photolysis instrument. This article reports a detailed study of the rates of hydroxide ion release from the excited XanOH using femtosecond pump−probe spectroscopy. The activation barrier for the XanOH excited-state heterolysis was evaluated by comparing the heterolysis rate constants in a series of acetonitrile (CH_3CN):water solvent mixtures with the corresponding thermodynamic Gibbs free energies obtained using the Förster cycle. The kinetic results are discussed and compared with the kinetics of proton release from known photoacids.

EXPERIMENTAL SECTION

Steady-State Spectroscopy. UV/vis absorption spectra were recorded on a Varian Cary 50 Bio spectrometer in a 1 cm quartz cell. The pK_{exp} values were determined as follows: XanOH (TCI America) was dissolved in an acetonitrile (Sigma-Aldrich)/water (Barnstead Nanopure system) mixture, and $HClO_4$ (Sigma-Aldrich) was added until the concentrations of Xan^+ and XanOH were equal (the concentration of Xan^+ was determined using the absorbance at 374 nm). The concentration of protons when $[Xan^+] = [XanOH]$ was determined by subtracting the initial concentration of $HClO_4$ (C_{in}) and the concentration of Xan^+:$[H^+] = C_{in} - [Xan^+]$.

Spectroelectrochemistry. Spectroelectrochemistry was performed using a Pt mesh working electrode, nonaqueous Ag/Ag^+ reference electrode, and Pt wire as an auxiliary electrode. The absorption spectra were recorded on a Varian Cary 50 Bio spectrometer, and the potential was provided by an EC Epsilon potentiostat. A solution of 1 mM Xan^+ in acetonitrile containing 0.1 M TBAP was degassed with argon (Ar) prior to each experiment. The changes in the absorption were monitored in 6 s intervals after applying a potential of −0.8 V vs Ag/Ag^+.

Femtosecond Transient Absorption Experiments. The 800 nm laser pulses were produced at a 1 kHz repetition rate by a mode-locked Ti:sapphire laser and regenerative amplifier (Hurricane, Spectra-Physics). The output from the Hurricane was split into pump (85%) and probe (10%) beams. The frequency of the pump beam was doubled and tripled using the second and third harmonic outputs from the SuperTripler (CSK) to obtain 266 and 400 nm excitation sources. The probe beam was focused into a horizontally moving CaF_2 crystal for white light continuum generation between 350 and 800 nm. The flow cell (Starna Cell Inc. 45-Q-2, 0.9 mL volume with 2 mm path length), pumped by a Variable Flow Mini-Pump (Control Company), was used to prevent photodegradation of the sample. After passing through the cell at the magic-angle geometry, the continuum was coupled into an optical fiber and input into a CCD spectrograph (Ocean Optics, S2000). The data acquisition was achieved using in-house LabVIEW (National Instruments) software routines. The group velocity dispersion of the probing pulse was determined using

dx.doi.org/10.1021/jp5080169 | J. Phys. Chem. B 2015, 119, 2498−2506

nonresonant optical Kerr effect (OKE) measurements.[37] Sample solutions were prepared at a concentration needed to have absorbance of 1.0 at the excitation wavelength.

Nanosecond Transient Absorption Experiments. A Nd:YAG laser (Spectra Physics LAB-150-10) was used as the excitation source with an excitation wavelength of 266 nm. All of the solutions utilized in these experiments were made such that the absorbance at 266 nm was 1. Transient absorption spectra were recorded using a Roper ICCD-Max 512T digital intensified CCD camera with up to 2 ns temporal resolution. The single wavelength kinetic measurements were recorded using a PMT connected to an oscilloscope, which was directly connected to a computer that runs a custom LabVIEW control and acquisition program.

Data Analysis. Transient absorption data were analyzed using a SPECFIT/32 Global Analysis System (Spectrum Software Associates, MA, USA). This program allows a decomposition of transient absorption data using kinetic models. The fitting process returns the predicted absorption spectra of individual colored species involved in the photochemical process along with their decay profiles. The analysis is achieved by a global analysis method that uses the singular value decomposition method to reduce the size of the fitted data.

RESULTS AND DISCUSSION

Thermodynamics. The ground-state conversion of XanOH to Xan^+ was studied using pH-dependent UV/vis absorption spectroscopy (Figure 1a). The dominant species in pH-neutral solution is XanOH (λ_{max} = 289 nm), while the C−O heterolysis takes place upon acidification, forming Xan^+ (λ_{max} = 450 nm), in consistency with previous literature reports.[30,34] The pH at which [XanOH] = [Xan^+] is 0.4. This value is referred to in the literature as the pK_{R+} value,[38−40] and it strongly correlates with the stability of the carbocation formed. Due to the significance of carbocations in organic reactions,[41] pK_{R+} values of many hydroxylated organic compounds have been experimentally determined,[38−40,42] and these data suggest that the pK_{R+} value (carbocation stability) depends on the delocalization of the positive charge in R^+, steric effects, differential solvation stabilization, and other factors.[43] For example, the pK_{R+} value of the triphenylmethyl cation[38] is −6.63, suggesting that Xan^+ is more stable than Ph_3C^+, due to increased planarity and positive charge delocalization.

The stability of Xan^+ relative to XanOH drastically increases in the singlet excited state, as is evident from the pK_{R+}^* = 28.2 value evaluated using the Förster cycle[34] (Figure 1b; ref 34 reports the pK_{R+}^* = 22.3 value for XanOH, possibly because the authors used a different value for the XanOH S_0−S_1 energy difference). The increased relative stability of Xan^+ in the S_1 state is also evident from the Gibbs free energies for the C−O heterolysis: XanOH → Xan^+ + OH^- (Figure 1b). In the ground state, the heterolysis is thermodynamically unfavorable (ΔG = +18.6 kcal/mol), while it becomes highly favorable in the S_1 state (ΔG^* = −19.3 kcal/mol). Since it is known that excited-state aromaticity follows the 4*n* rule, while the ground-state aromaticity follows the 4*n* + 2 rule,[44,45] we propose that Xan^+ topology favors the stabilization by the 4*n* resonance structure. For instance, Xan^+ is an aromatic 14-π-electron system if the lone electron pair from the oxygen atom is counted. However, if the oxygen atom in excited Xan^+ were less prone to donate its electron pair, the molecule would become a 12-π-electron antiaromatic system. Similar but less drastic changes in ground- vs excited-state reactivity were observed in photoacids, where pK_a values change up to 12 orders of magnitude upon electronic excitation.[16−18]

The article is focused on evaluating the activation barrier for the hydroxide ion release from XanOH. For this purpose, the equilibrium constant for the hydroxide ion release was tuned using acetonitrile/water solvent mixtures. The reaction of interest is

$$\mathrm{XanOH} \rightleftharpoons \mathrm{Xan^+} + \mathrm{OH^-} \qquad K_{OH} = \frac{[\mathrm{Xan^+}][\mathrm{OH^-}]}{[\mathrm{XanOH}]} \tag{1}$$

The K_{OH} values in various acetonitrile/water mixtures were obtained by experimentally determining the equilibrium constant K_{exp}:

$$\mathrm{XanOH} + \mathrm{H_3O^+} \rightleftharpoons \mathrm{Xan^+} + 2\mathrm{H_2O} \qquad K_{exp} = \frac{[\mathrm{Xan^+}]}{[\mathrm{XanOH}][\mathrm{H_3O^+}]} \tag{2}$$

K_{exp} values in solvent mixtures were obtained by titrating the perchloric acid into the XanOH solution and by using UV/vis absorption spectroscopy to obtain the equilibrium concentrations of Xan^+ and XanOH. The link between K_{exp} and K_{OH} was obtained using the water ionization constant in water/acetonitrile mixtures:

$$2\mathrm{H_2O} \rightleftharpoons \mathrm{H_3O^+} + \mathrm{OH^-} \qquad K_w^m = [\mathrm{H_3O^+}][\mathrm{OH^-}] \tag{3}$$

While K_w is well-known in purely aqueous solution, the evaluation of K_w in a series of acetonitrile/water mixtures is not straightforward. In water/organic solvent mixtures, the ionization of both solvents needs to be considered and the constant obtained using this approach represents the solvent autoprotolysis constant, K_{ap}, not the ionization constant for water, K_w.[46,47] For simplicity, we will assume that only water undergoes autoprotolysis in all water/acetonitrile mixtures studied in this work. This assumption is justified considering that the pK_{ap} of pure water is 14.00, while the pK_{ap} of pure acetonitrile is 33.58.[48]

The K_w value will vary in different water/acetonitrile mixtures. It was previously shown that the water ionization constant in organic solvent/water mixtures (pK_w^m) can be expressed as[49]

$$pK_w^m = pK_w^{H_2O} \cdot \chi_{H_2O} + pK_w^{CH_3CN} \cdot \chi_{CH_3CN} \tag{4}$$

where $pK_w^{H_2O}$ is the ionization constant of water in pure water ($pK_w^{H_2O}$ = 14.00), while $pK_w^{CH_3CN}$ is the ionization constant of water in pure acetonitrile ($pK_w^{CH_3CN}$ = 19.95). The coefficients χ_{H_2O} and χ_{CH_3CN} are the mole fractions of water and acetonitrile, respectively. We used the values for pK_w^m and K_{exp} to derive the constants for ground-state hydroxide release $K_{OH} = K_w^m \cdot K_{exp}$. Furthermore, the equilibrium constants for excited-state hydroxide ion release (K_{OH}^*) were obtained using the Förster cycle.

The ground-state heterolysis of XanOH is thermodynamically unfavorable in all acetonitrile/water mixtures, while it becomes favorable in the excited state (Figure 2 and Table 1). The pK value changes by ∼28 units upon excitation, indicating that XanOH can be considered as a "super"-photobase, in analogy to the corresponding "super"-photoacids.[16,17] The increasing amounts of acetonitrile in the solvent mixture result in a decreased tendency toward heterolysis in both the ground

dx.doi.org/10.1021/jp5080169 | J. Phys. Chem. B 2015, 119, 2498−2506

Table 1. Thermodynamic Parameters for XanOH in Acetonitrile/Water Mixtures

mole % CH_3CN	pK_w^m	pK_{exp}	pK_{OH}	ΔG_{OH} (kcal/mol)	pK_{OH}*	ΔG_{OH}* (kcal/mol)
0.0052	14.03	−0.24	13.79	18.81	−14.00	−19.09
0.0159	14.09	−0.54	13.55	18.48	−14.24	−19.41
0.0215	14.13	−0.40	13.73	18.72	−14.06	−19.18
0.0638	14.38	−0.63	13.75	18.75	−14.04	−19.14
0.2200	15.31	−0.33	14.98	20.43	−12.81	−17.47
0.5080	17.02	−0.33	16.69	22.76	−11.10	−15.14
0.7820	18.65	−0.73	17.92	24.44	−9.87	−13.46

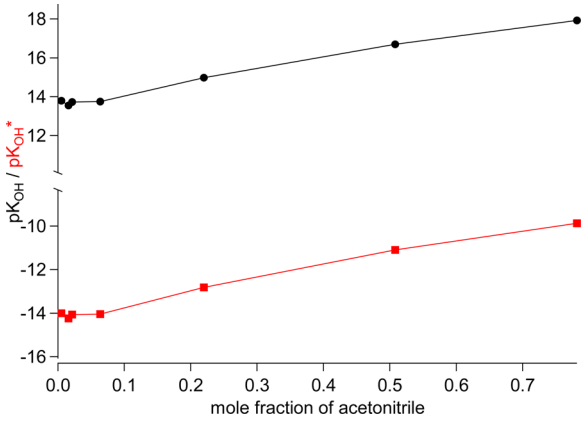

Figure 2. Variation of pK_{OH} (black) and pK_{OH}* (red) for XanOH as a function of acetonitrile content in water.

and excited states. This decrease is consistent with poorer solvation of Xan^+ and OH^- ions in solvents with lower dielectric constant (ε_{H_2O} = 80.10, ε_{CH_3CN} = 36.62 at 20 °C).[50]

Kinetics. The dynamics of XanOH excited-state heterolysis were studied using ultrafast pump−probe spectroscopy. In pure acetonitrile, the S_1 state of XanOH exhibits a broad absorption spectrum in the visible range (Figure 3a, red trace). As time evolves, the S_1 state decays and a new transient with absorption in the 350−600 nm range is formed. The conversion is seen more clearly from the spectra of principal components obtained using global analysis (Figure 3b). To identify the origin of this new transient, the spectra of possible products are shown in Figure 3c: (i) Xan^+ cation, which would be formed if XanOH heterolysis took place; (ii) Xan• radical, which would be formed if XanOH homolysis took place, and (iii) T_1 state of XanOH, which would be formed if intersystem crossing took place. The spectrum of Xan• radical was obtained by electrochemical reduction of Xan^+ cation at −0.8 V vs Ag/Ag^+, while the spectrum of the T_1 state was obtained using nanosecond transient absorption and is consistent with the previous literature report.[29] By comparing the spectrum of the intermediate formed in pump−probe experiment with the spectra of species in Figure 3c, we conclude that the S_1 state of XanOH undergoes intersystem crossing in acetonitrile to form the T_1 state. The estimated lifetime of the XanOH S_1 state is 2.4 ns. Thus, the heterolytic OH^- release does not take place in pure acetonitrile because the kinetics of heterolysis is too slow to compete with the intersystem crossing. The T_1 state of XanOH in acetonitrile undergoes homolytic C−O bond cleavage to generate the Xan• radical, as reported previously.[29]

As the amount of water in acetonitrile is increased, the heterolytic C−O bond cleavage is fast enough to compete with

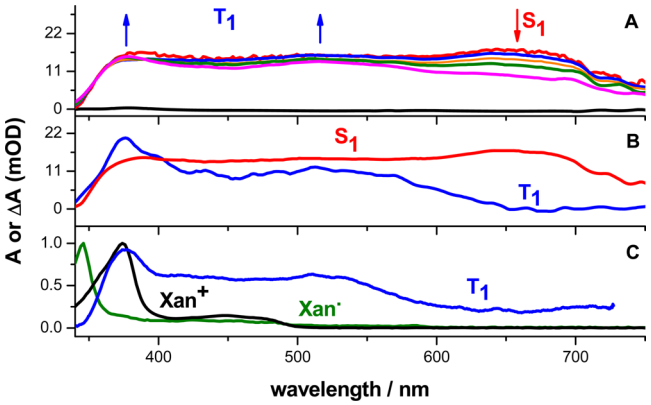

Figure 3. Excited-state behavior of XanOH in pure acetonitrile. (A) Femtosecond transient absorption spectra obtained at −5 (black), 3 (red), 50 (blue), 400 (orange), 850 (green), 1370 (pink) ps time intervals after the 266 nm excitation pulse. (B) The principal component spectra obtained using the global analysis of the transient absorption data. (C) Absorption spectra of Xan^+, Xan•, and the T_1 state of XanOH. Solvent: CH_3CN. The spectrum of Xan• was obtained using electrochemical reduction of Xan^+ at −0.8 V vs Ag/Ag^+. The spectrum of the XanOH T_1 state was obtained using nanosecond transient absorption (excitation at 266 nm; time delay 10 ns).

intersystem crossing, as can be seen from the transient absorption spectra obtained in the 1:1 (volume) water/acetonitrile mixture (Figure 4a). The decay of the S_1 state is

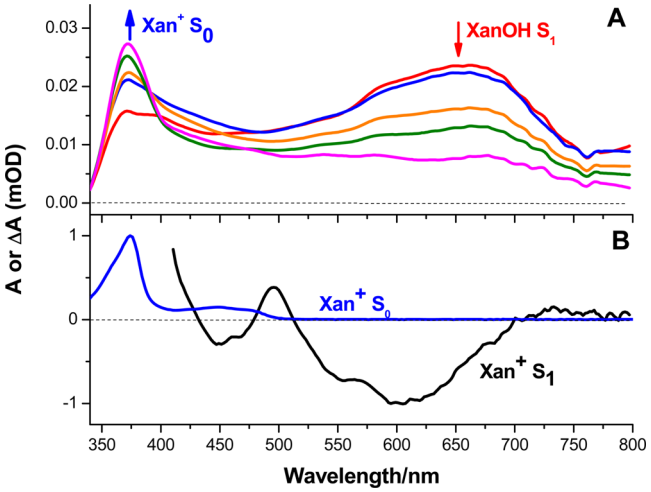

Figure 4. Excited-state behavior of XanOH in acetonitrile/water mixture (χ_{CH_3CN} = 0.256). (A) Femtosecond transient absorption spectra obtained at −5 (black), 3 (red), 64 (blue), 400 (orange), 820 (green), and 1370 (pink) ps time intervals after the 266 nm excitation pulse. (B) Absorption spectra of Xan^+ in S_0 and S_1 states. The spectrum of the Xan^+ S_1 state was obtained using femtosecond transient absorption (excitation at 400 nm; time delay 1 ns).

accompanied by an increase of the absorption at 374 nm, which is assigned to the S_0 state of the Xan^+ cation. A small fraction of the S_1 state undergoes intersystem crossing, as is evident from the growth of XanOH T_1 state absorption in the 500−600 nm range.

Previous studies of XanOH photoheterolysis have shown that the process occurs adiabatically, since the fluorescence from Xan^+ was observed upon excitation of XanOH.[30] Our

dx.doi.org/10.1021/jp5080169 | J. Phys. Chem. B 2015, 119, 2498−2506

transient absorption data do not show evidence for the adiabatic pathway. The excited-state absorption spectrum of Xan^+ (Figure 4b) exhibits three features: ground-state bleach below 500 nm, excited-state absorption at 500 nm, and stimulated emission above 500 nm. If the S_1 state of Xan^+ is formed adiabatically from XanOH, one would expect to observe the excited-state absorption and stimulated emission bands, while the ground-state bleach at 450 nm would not be present. Since the transient absorption spectra of XanOH (Figure 4a) do not exhibit stimulated emission above 500 nm, we conclude that the predominant heterolysis pathway involves a diabatic process to form Xan^+ in the S_0 state. Since the detection limit of our pump−probe instrument is much lower than that of the fluorescence spectroscopy reported by Wan et al.,[30] it is likely that the adiabatic pathway occurs with a very low yield. This is consistent with the study reported by Das, who reports that 99% of the photogenerated Xan^+ evolves directly into the ground state.[29]

The transient absorption signal in the 650−750 nm region originates mostly from the S_1 state of XanOH. Thus, the 650 nm wavelength was used to obtain the rates of XanOH excited-state heterolysis at different water/acetonitrile mixtures (Figure 5). The lifetime of the S_1 state gradually decreases as the water

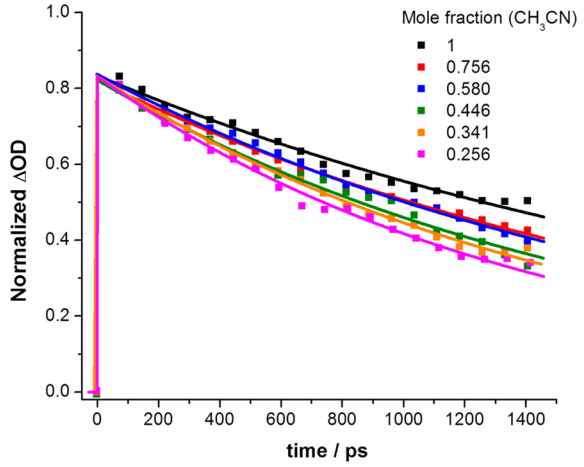

Figure 5. Normalized kinetic traces of XanOH in different water/acetonitrile mixtures. Pump wavelength, 266 nm; probe wavelength, 650 nm.

content is increased, due to an increased rate of heterolysis. The decay was fitted using a single exponential function, and the fitted k_{exp} values are listed in Table 2. In pure acetonitrile, the heterolysis does not occur and the observed rate corresponds to the rate of intersystem crossing: $k_{exp} = k_{isc}$. In other solvent mixtures, the observed rate represents a sum of intersystem crossing and heterolysis rates: $k_{exp} = k_{OH} + k_{isc}$. Assuming that the rate of intersystem crossing remains constant in all solvent mixtures, the rate of heterolysis k_{OH} was obtained by subtraction (Table 2).

Table 2. Kinetic Parameter for XanOH in Water/Acetonitrile Mixtures

mole fraction CH_3CN	ΔG^* (kcal/mol)	k_{exp} (s^{-1})	k_{OH} (s^{-1})
1	−11.56	4.09×10^8	$\ll 4.09 \times 10^8$
0.756	−13.46	4.90×10^8	0.81×10^8
0.580	−14.84	5.17×10^8	1.08×10^8
0.446	−15.88	5.85×10^8	1.76×10^8
0.341	−16.70	6.33×10^8	2.24×10^8
0.256	−17.36	7.00×10^8	2.91×10^8

Activation Barrier. The rate constants of group transfer reactions (such as electron, proton, hydrogen-atom, or methyl transfers) are often related to the energy barrier using the well-known transition state theory expression:

$$k = A \cdot e^{-(\Delta G^{\#}/R \cdot T)} \tag{5}$$

where $\Delta G^{\#}$ is the Gibbs free energy for the transition state and A is the pre-exponential factor. To predict the rate of a given reaction, one needs to determine how $\Delta G^{\#}$ depends on a parameter that is readily obtainable experimentally (such as the driving force of the reaction, ΔG°), which is often a significant challenge.

To develop a suitable theory, one needs to determine the characteristic reaction coordinate (RC) along which the reactants are brought to the product states. In the case of electron transfer reaction, Marcus has shown that the dominant rate-determining factor is the solvent polarization response to the charge distribution changes that occur as the electron hops from the donor to the acceptor.[51−53] The reaction proceeds along the solvent RC, and the free energy correlation is expressed as

$$\Delta G^{\#} = \left(1 + \frac{\Delta G^{\circ}}{4 \cdot \Delta G_o^{\#}}\right)^2 \cdot \Delta G_o^{\#} \tag{6}$$

where $\Delta G_o^{\#}$ is the activation energy for the symmetric transfer ($\Delta G^{\circ} = 0$). The counterintuitive outcome of the Marcus expression is the existence of the "inverted region", where the reaction rate decreases with increasing driving force (red traces in Figure 6). This theory was shown experimentally to be valid for numerous electron transfer processes.[51,54,55]

When one moves toward more complex reactions, such as proton transfer, it is no longer clear whether the RC is in the solvent. The proton transfer occurs in a strong coupling regime, where the bond stretching and compression is expected to greatly contribute to the reaction rate. The theory that

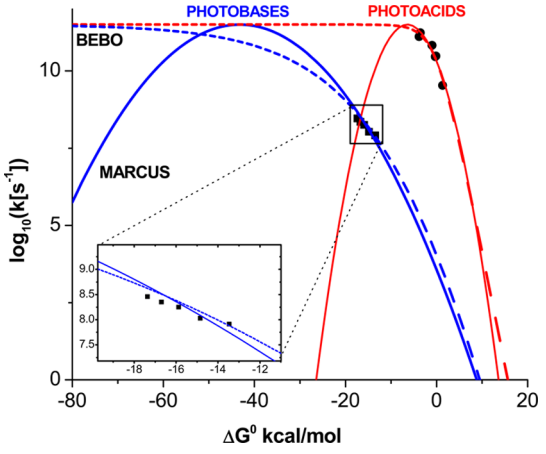

Figure 6. Free-energy correlation for OH^- release from XanOH. Black squares represent the data obtained in this study. The blue solid curve is a fit obtained by the Marcus model (eq 6, $A = 10^{11.5}$, $\Delta G_o^{\#} = 10.80$), while the blue dashed curve represents a fit obtained using the BEBO model (eq 7, $A = 10^{11.5}$, $\Delta G_o^{\#} = 10.17$). For comparison, the red curves represent the Marcus (solid line) and BEBO (dashed line) fits obtained from the photoacid studies in ref 61 ($A = 10^{11.5}$, $\Delta G_o^{\#} = 1.6$).

dx.doi.org/10.1021/jp5080169 | J. Phys. Chem. B 2015, 119, 2498−2506

describes the behavior of such reactions is the bond-energy bond-order (BEBO) theory, originally developed for gas-phase reactions.[56−60] The BEBO takes advantage of the fact that the bond energy is an almost linear function of the bond order. As one goes from reactants to the product, the energy is evaluated as a linear combination of the reactant and product energies, scaled by their bond order at a given point along the reaction coordinate. According to the BEBO model, the $\Delta G_o^{\#}$ is expected to depend on the driving force as

$$\Delta G^{\#} = \frac{\Delta G^{\circ}}{2} + \Delta G_o^{\#} + \frac{\Delta G_o^{\#}}{\ln 2} \ln\left(\cosh\left(\frac{\Delta G^{\circ} \ln 2}{2\Delta G_o^{\#}}\right)\right) \quad (7)$$

Unlike the Marcus treatment, the BEBO theory predicts the rate to level off at high driving forces (blue traces in Figure 6). However, at low driving forces, both theories predict the same free energy−reactivity relationship.

In the case of proton transfer reactions in the condensed phase, it is still not clear which of the two theories holds. All experimentally obtained values so far lie in the "normal region", where both theories predict a similar outcome. For example, Figure 6 shows the Marcus and BEBO plots for the proton transfer reactions obtained by Nibbering.[61] Experimental values were obtained in the pK_a range from −4 to +3, which belong to the region where both Marcus and BEBO exhibit similar behavior. To determine whether the solvent or molecular coordinate is the predominant reaction coordinate in the proton transfer reaction, one would need to experimentally access the "inverted region", where thermodynamic driving forces are large, which has not yet been accomplished. It is interesting to note, however, that some computational studies predict that the solvent reorganization could be the predominant RC.[62]

In the case of hydroxide ion transfer studied here, the thermodynamic driving forces are much higher than those of a typical proton transfer reaction. While all photoacids studied so far exhibit pK_a values that are more positive than −10,[17,61] the pK_{OH}* values of XanOH in solvent mixtures are in the −15 to −10 range, which could possibly allow the access to the desired inverted region, as long as the activation parameters for OH^- transfer are similar to those of the proton transfer. Unfortunately, we find here that the activation parameters are not the same and that the observed rates are still in the normal regime.

The black squares in Figure 6 show how our experimental OH^- release rates depend on the driving force. One question is whether it is justifiable to relate the observed rates with the driving force for the adiabatic OH^- release, even though we have shown earlier in this article that 99% of the reaction proceeds nonadiabatically, to the ground state Xan^+. The reaction can be considered to occur in two steps: (i) adiabatic excited-state OH^- release along the RC for OH^- transfer; (ii) the S_1/S_0 decay via a conical intersection (CI) that is reached along a different RC, after the transition state for OH^- release is crossed. Here, we assume that the activation energy for OH^- release is higher than the barrier for the S_1/S_0 deactivation and that the "bottle-neck" for the reaction is the OH^- ion release along the S_1 potential energy surface. Our assumption is justified by the fact that the rate correlates well with the driving force for the adiabatic OH^- release, which is not likely to be the case if the rate-determining step is along the S_1/S_0 deactivation RC.

The observed rates increase with the driving force, which suggests that the Marcus inverted (or BEBO level-off) region is not reached, even though systems with high driving forces were used. This result suggests that the energy barrier for OH^- transfer is significantly higher than the barrier for the proton transfer. Indeed, the fitted curves (assuming log(A) = 11.5, which is consistent with the value used previously for the proton transfer[61]) gave $\Delta G_o^{\#}$ values of 10.17 kcal/mol (using BEBO model) and 10.80 kcal/mol (using Marcus expression). These values are significantly higher than those obtained from the photoacid studies, where $\Delta G_o^{\#}$ values were in the 1−4 kcal/mol range.[18,61,63] The following text discusses the possible reasons for the observed differences in the H^+ and OH^- transfer barriers.

It is possible that the activation barrier for OH^- release involves predominately the solvent reorganization. While we cannot evaluate the solvent reorganization energy for OH^- release, it might be useful to evaluate the magnitude of the reorganization energy for the hypothetical electron transfer process in the same solvent mixtures. The solvent reorganization energy λ_s (in J/mol) for electron transfer processes is usually evaluated using the following expression:

$$\lambda_s = \frac{e^2}{4\pi\varepsilon_0}\left(\frac{1}{2r_D} + \frac{1}{2r_A} - \frac{1}{r}\right)\left(\frac{1}{\varepsilon_{op}} - \frac{1}{\varepsilon_s}\right)\cdot N_A \quad (8)$$

where e is the elementary charge, ε_0 is the vacuum permittivity, r_D and r_A represent the donor and acceptor radii, and r is the distance between the donor and the acceptor. The ε_{op} and ε_s are optical and static dielectric constants. If all of the activation energy arises due to solvent reorganization, $\Delta G_o^{\#}$ can be estimated as $\lambda_s/4$. Assuming that the donor and acceptor radii are 3 Å each, the $\Delta G_o^{\#}$ at the contact distance is evaluated as 7.4 kcal/mol in acetonitrile and 7.6 kcal/mol in water. This value is lower than the experimentally obtained reorganization energy for the OH^- transfer, indicating that the simple continuum model for the solvent reorganization energy does not reproduce our experimental findings. In the case of OH^- transfer, the process is expected to occur along a preformed hydrogen-bonded complex, which is not captured by the continuum model used in eq 8. Similar effects were observed in proton transfer reactions of various photoacids, which are known to occur via hydrogen-bonded complexes.[64−66] Given that the $\Delta G_o^{\#}$ value observed in this work is higher than that evaluated for solvent reorganization energy for a simple charge transfer process, we postulate that the RC for OH^- transfer reactions involves the solvent and molecular reorganization within a preformed H-bonded complex.

If solvent is modeled as a simple dielectric continuum without considerations of specific solvent−solute interactions, the solvent reorganization energy is expected to be similar for both H^+ and OH^- transfers. However, H^+ transfers are generally very fast and limited by the solvent reorganization, while the OH^- transfer reported here seems to be slower and controlled by the internal RC. A possible reason for the difference in reactivity might be due to the tunneling effects. In proton transfer reactions that occur with moderate rates (such as proton transfer to or from carbon atoms, where hydrogen bonds cannot be formed), proton tunneling was found to take place, causing fast proton transfer rates even in systems with activation barriers as high as 10 kcal/mol.[67] In the case of OH^- transfer, such tunneling effects are not expected to take place, suggesting that, given the same energy barrier, the observed

dx.doi.org/10.1021/jp5080169 | J. Phys. Chem. B 2015, 119, 2498−2506

Scheme 1. Proposed Transition State Structure for H^+ and OH^- Release from Photoacids and Photobases

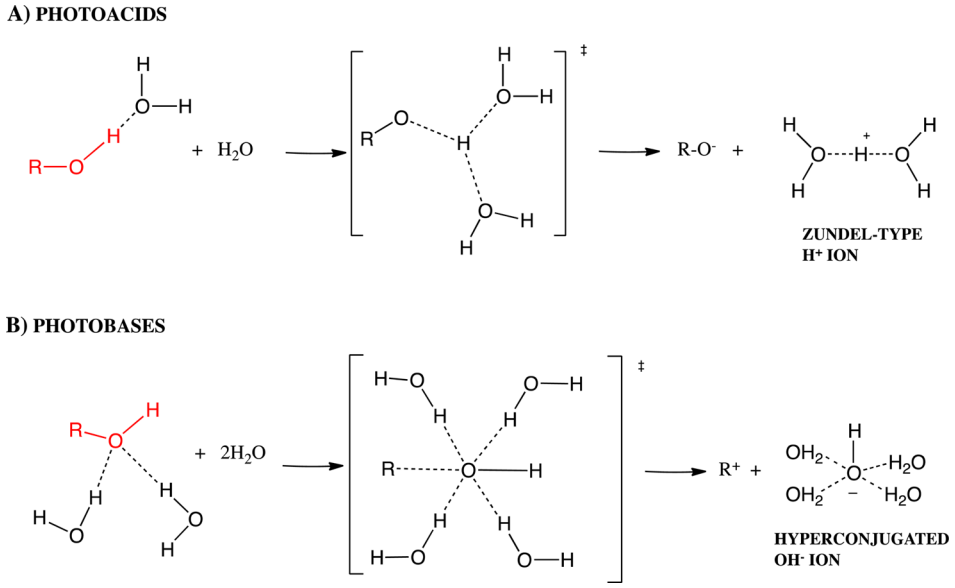

rates for OH^- transfer will generally be lower than the proton transfer rates.

The higher intrinsic barrier observed for OH^- release relative to that for H^+ transfer might also originate from the differences in the structures of solvated ions, which cause the transition state for OH^- release to be more ordered (entropically unfavored). It is intriguing that the observed rates of OH^-/H^+ ion transfer in photobases/photoacids seems to correlate with the known rates of OH^-/H^+ migration in water: in both cases, the rate of H^+ transfer/migration is faster than the observed rate of OH^- transfer/migration. This similar trend could be due to the differences in the structures of solvated H^+ and OH^- ions. Since most currently known excited-state transfers of H^+ and OH^- ions occur in the presence of protic solvents,[17,18,20,28,61] it is likely that the specific solvation via hydrogen bonds plays an important role in the dynamics of the H^+/OH^- transfer. While the structure and dynamics of solvated H^+ and OH^- ions are still an active area of research,[7,10,14,15,68] the current status in the field suggests that the two species exhibit significantly different structures in aqueous environment: while aqueous H^+ ions tend to adopt Eigen- and Zundel-type structures,[18,68] the OH^- ion is considered to be hyperconjugated, with an oxygen atom of the OH^- ion forming a square-planar hydrogen-bonded structure with four water molecules.[10,11] The lower rate of OH^- migration in water relative to H^+ migration is thought to occur due to the fact that the hyperoconjugated anion cannot readily accept another proton.[10,69] The fact that the solvated OH^- requires hyperconjugation might cause a larger entropic barrier for the transition state in the case of photobases (Scheme 1). As a simplified example, the proton transfer from the photoacids is likely to occur via a readily available Zundel-type transition state (Scheme 1a). On the other hand, the transition state for the OH^- ion release from photobases might require steric crowding to generate a hyperconjugated aqueous OH^- ion (Scheme 1b).

The hydroxide transfer reactions are also relevant to the chemical[70−72] and biochemical[73−75] hydrolysis of amides and esters. The first step of these hydrolysis reactions is the attack of the hydroxide ion to the carbonyl group, which is generally considered to generate a tetrahedral intermediate (TI). The TI is short-lived but has been detected in some cases using NMR and X-ray spectroscopy.[73,76,77] We evaluated the $\Delta G_o^{\#}$ values from the previously reported barriers for the generation of TI, and we find that they are similar to our range of $\Delta G_o^{\#}$ = 10.17−10.80 kcal/mol.[72] For example, the intrinsic barriers for the TI formation during the attack of OH^- to the series of carbonyl compounds are in the 10−15 kcal/mol range.[72,78] This similarity in $\Delta G_o^{\#}$ values suggests that the transition state structures in these reactions are stabilized/destabilized by common factors.

CONCLUSIONS

Photochemical reactions are limited relative to their ground-state analogues, due to the short lifetimes of most molecules in their excited state. Within several nanoseconds or microseconds, the excited molecule has only a limited number of attempts to adopt a favorable reactive conformation. Thus, most photochemical events involve simple transfers of electrons or protons, even though many other processes would be thermodynamically favorable. To explore other photochemical transfer reactions, we report here a study of photochemical hydroxide ion transfer from the model alcohol XanOH to the solvent. We find that the intrinsic barrier for the reaction ($\Delta G_o^{\#}$ = 10.17−10.80 kcal/mol) is significantly higher from the barriers reported previously for electron and proton transfer reactions. While we currently do not understand the reason for slower kinetics, it is intriguing that the same trend can be found in the diffusion of H^+ and OH^- ions in aqueous medium: H^+ ions diffuse 2 times faster than OH^- ions, and this difference is attributed to different solvation of the two ions. In analogy, we postulate that the slower OH^- transfer kinetics presented here are due to the higher energetic requirements to hypersolvate the OH^- ion.

AUTHOR INFORMATION

Notes

The authors declare no competing financial interest.

dx.doi.org/10.1021/jp5080169 | J. Phys. Chem. B 2015, 119, 2498−2506

■ ACKNOWLEDGMENTS

This work was supported by National Science Foundation (CHE-1055397 CAREER award to K.D.G.).

■ REFERENCES

(1) Mulkidjanian, A. Y.; Heberle, J.; Cherepanov, D. A. Protons @ Interfaces: Implications for Biological Energy Conversion. *Biochim. Biophys. Acta* **2006**, *1757*, 913−930.
(2) Caldin, E.; Gold, V. *Proton-Transfer Reactions*; Chapman and Hall: London, 1975.
(3) Kreuer, K.-D. Ion Conducting Membranes for Fuel Cells and Other Electrochemical Devices. *Chem. Mater.* **2013**, *26*, 361−380.
(4) Atkins, P.; Paula, J. d. *Atkins' Physical Chemistry*, 7th ed.; Oxford University Press: Oxford, U.K., 2002.
(5) Asmis, K. R.; Pivonka, N. L.; Santambrogio, G.; Brümmer, M.; Kaposta, C.; Neumark, D. M.; Wöste, L. Gas-phase Infrared Spectrum of the Protonated Water Dimer. *Science* **2003**, *299*, 1375−1377.
(6) Meiboom, S. Nuclear Magnetic Resonance Study of the Proton Transfer in Water. *J. Chem. Phys.* **2004**, *34*, 375−388.
(7) Woutersen, S.; Bakker, H. J. Ultrafast Vibrational and Structural Dynamics of the Proton in Liquid Water. *Phys. Rev. Lett.* **2006**, *96*, 138305−138309.
(8) Hassanali, A.; Giberti, F.; Cuny, J.; Kühne, T. D.; Parrinello, M. Proton Transfer Through the Water Gossamer. *Proc. Natl. Acad. Sci. U.S.A.* **2013**, *110*, 13723−13728.
(9) Voth, G. A. Computer Simulation of Proton Solvation and Transport in Aqueous and Biomolecular Systems. *Acc. Chem. Res.* **2006**, *39*, 143−150.
(10) Marx, D.; Chandra, A.; Tuckerman, M. E. Aqueous Basic Solutions: Hydroxide Solvation, Structural Diffusion, and Comparison to the Hydrated Proton. *Chem. Rev.* **2010**, *110*, 2174−2216.
(11) Tuckerman, M. E.; Marx, D.; Parrinello, M. The Nature and Transport Mechanism of Hydrated Hydroxide Ions in Aqueous Solution. *Nature* **2002**, *417*, 925−929.
(12) Botti, A.; Bruni, F.; Imberti, S.; Ricci, M.; Soper, A. Solvation of Hydroxyl Ions in Water. *J. Chem. Phys.* **2003**, *119*, 5001−5004.
(13) Megyes, T.; Bálint, S.; Grósz, T.; Radnai, T.; Bakó, I.; Sipos, P. The Structure of Aqueous Sodium Hydroxide Solutions: a Combined Solution X-ray Diffraction and Simulation Study. *J. Chem. Phys.* **2008**, *128*, 044501.
(14) Roberts, S. T.; Petersen, P. B.; Ramasesha, K.; Tokmakoff, A.; Ufimtsev, I. S.; Martinez, T. J. Observation of a Zundel-like Transition State During Proton Transfer in Aqueous Hydroxide Solutions. *Proc. Natl. Acad. Sci. U.S.A.* **2009**, *106*, 15154−15159.
(15) Roberts, S. T.; Ramasesha, K.; Petersen, P. B.; Mandal, A.; Tokmakoff, A. Proton Transfer in Concentrated Aqueous Hydroxide Visualized Using Ultrafast Infrared Spectroscopy. *J. Phys. Chem. A* **2011**, *115*, 3957−3972.
(16) Tolbert, L. M.; Haubrich, J. E. Photoexcited Proton Transfer from Enhanced Photoacids. *J. Am. Chem. Soc.* **1994**, *116*, 10593−10600.
(17) Tolbert, L. M.; Solntsev, K. M. Excited-state Proton Transfer: from Constrained Systems to "Super" Photoacids to Superfast Proton Transfer. *Acc. Chem. Res.* **2002**, *35*, 19−27.
(18) Agmon, N. Elementary Steps in Excited-state Proton Transfer. *J. Phys. Chem. A* **2005**, *109*, 13−35.
(19) Rini, M.; Magnes, B.-Z.; Pines, E.; Nibbering, E. T. Real-time Observation of Bimodal Proton Transfer in Acid-base Pairs in Water. *Science* **2003**, *301*, 349−352.
(20) Mohammed, O. F.; Pines, D.; Dreyer, J.; Pines, E.; Nibbering, E. T. Sequential Proton Transfer Through Water Bridges in Acid-base Reactions. *Science* **2005**, *310*, 83−86.
(21) Hansen, J. E.; Pines, E.; Fleming, G. R. Excited-state Proton Transfer of Protonated 1-Aminopyrene Complexes with. beta.-Cyclodextrin. *J. Phys. Chem.* **1992**, *96*, 6904−6910.
(22) Cohen, B.; Huppert, D.; Solntsev, K. M.; Tsfadia, Y.; Nachliel, E.; Gutman, M. Excited State Proton Transfer in Reverse Micelles. *J. Am. Chem. Soc.* **2002**, *124*, 7539−7547.
(23) Sedgwick, M.; Cole, R. L.; Rithner, C. D.; Crans, D. C.; Levinger, N. E. Correlating Proton Transfer Dynamics to Probe Location in Confined Environments. *J. Am. Chem. Soc.* **2012**, *134*, 11904−11907.
(24) Spry, D.; Goun, A.; Glusac, K.; Moilanen, D. E.; Fayer, M. Proton Transport and the Water Environment in Nafion Fuel Cell Membranes and AOT Reverse Micelles. *J. Am. Chem. Soc.* **2007**, *129*, 8122−8130.
(25) Wan, P.; Shukla, D. Utility of Acid-Base Behavior of Excited States of Organic Molecules. *Chem. Rev.* **1993**, *93*, 571−584.
(26) Irie, M. Light-induced Reversible pH Change. *J. Am. Chem. Soc.* **1983**, *105*, 2078−2079.
(27) Liu, H.; Xu, Y.; Li, F.; Yang, Y.; Wang, W.; Song, Y.; Liu, D. Light-Driven Conformational Switch of i-Motif DNA. *Angew. Chem., Int. Ed.* **2007**, *46*, 2515−2517.
(28) Zhou, D.; Khatmullin, R.; Walpita, J.; Miller, N. A.; Luk, H. L.; Vyas, S.; Hadad, C. M.; Glusac, K. D. Mechanistic Study of the Photochemical Hydroxide Ion Release from 9-Hydroxy-10-methyl-9-phenyl-9, 10-dihydroacridine. *J. Am. Chem. Soc.* **2012**, *134*, 11301−11303.
(29) Minto, R. E.; Das, P. K. Laser Flash Photolysis Study of Photodehydroxylation Phenomena of 9-Phenylxanthen-9-ol and Photobehavior of Related Intermediates. Enhanced Electrophilicity of 9-Phenylxanthenium Cation Singlet. *J. Am. Chem. Soc.* **1989**, *111*, 8858−8866.
(30) Wan, P.; Yates, K.; Boyd, M. K. Adiabatic Photodehydroxylation of 9-Phenylxanthen-9-ol. Observation of Carbocation Fluorescence in Neutral Aqueous Solution. *J. Org. Chem.* **1985**, *50*, 2881−2886.
(31) McClelland, R. A.; Mathivanan, N.; Steenken, S. Laser Flash Photolysis of 9-Fluorenol. Production and Reactivities of the 9-Fluorenol Radical Cation and the 9-Fluorenyl Cation. *J. Am. Chem. Soc.* **1990**, *112*, 4857−4861.
(32) Cozens, F.; Li, J.; McClelland, R. A.; Steenken, S. Cyclohexadienyl-Type Cationic Intermediates in the Friedel−Crafts Alkylation of Benzene Derivatives with the 9-Fluorenyl Cation—Observation by Laser Flash Photolysis. *Angew. Chem., Int. Ed.* **1992**, *31*, 743−745.
(33) Wen, L.; Ma, J.; Tian, Y.; Zhai, J.; Jiang, L. A Photo-induced, and Chemical-Driven, Smart-Gating Nanochannel. *Small* **2012**, *8*, 838−842.
(34) Feldman, M. R.; Thame, N. G. Stabilities of Trivalent Carbon Species. 5. Equilibriums of Excited Singlet Alcohols and Carbocations. *J. Org. Chem.* **1979**, *44*, 1863−1865.
(35) Gurzadyan, G. G.; Steenken, S. Solvent-Dependent C− OH Homolysis and Heterolysis in Electronically Excited 9-Fluorenol: The Life and Solvation Time of the 9-Fluorenyl Cation in Water. *Chem.—Eur. J.* **2001**, *7*, 1808−1815.
(36) Okuyama, T.; Ueno, K.; Okuyama, T.; Ueno, K.; Morishima, Y.; Kamachi, M.; Fueno, T. Ion-pair Recombination of a Carbocation and Hydroxide Ion Observed in Solvolytic Media by Laser Photolysis of 9-Aryl-9-xanthenol. *Chem. Lett.* **1990**, 1129−1132.
(37) Yamaguchi, S.; Hamaguchi, H. O. Convenient Method of Measuring the Chirp Structure of Femtosecond White-light Continuum Pulses. *Appl. Spectrosc.* **1995**, *49*, 1513−1515.
(38) Deno, N.; Jaruzelski, J.; Schriesheim, A.; Carbonium Ions, I. An Acidity Function (C_0) Derived from Arylcarbonium Ion Equilibria. *J. Am. Chem. Soc.* **1955**, *77*, 3044−3051.
(39) Ito, S.; Morita, N.; Asao, T. Syntheses of Azulene Analogues of Triphenylmethyl Cation: Extremely Stable Hydrocarbon Carbocations and the First Example of a One-Ring Flip as the Threshold Rotation Mechanism for Molecular Propellers. *Bull. Chem. Soc. Jpn.* **1995**, *68*, 1409−1436.
(40) Zhang, X.-M.; Bruno, J. W.; Enyinnaya, E. Hydride Affinities of Arylcarbenium Ions and Iminium Ions in Dimethyl Sulfoxide and Acetonitrile. *J. Org. Chem.* **1998**, *63*, 4671−4678.
(41) Olah, G. A. Carbocations and Electrophilic Reactions. *Angew. Chem., Int. Ed.* **1973**, *12*, 173−212.

(42) Bunting, J. W.; Norris, D. J. Rates and Equilibriums for Hydroxide Ion Addition to Quinolinium and Isoquinolinium Cations. *J. Am. Chem. Soc.* **1977**, *99*, 1189−1196.
(43) Richard, J. P.; Amyes, T. L.; Toteva, M. M. Formation and Stability of Carbocations and Carbanions in Water and Intrinsic bBarriers to Their Reactions. *Acc. Chem. Res.* **2001**, *34*, 981−988.
(44) Baird, N. C. Quantum Organic Photochemistry. II. Resonance and Aromaticity in the Lowest $^3\pi\pi^*$ State of Cyclic Hydrocarbons. *J. Am. Chem. Soc.* **1972**, *94*, 4941−4948.
(45) Ottosson, H. Organic Photochemistry: Exciting Excited-state Aromaticity. *Nat. Chem.* **2012**, *4*, 969−971.
(46) Mussini, T.; Covington, A.; Longhi, P.; Rondinini, S. Criteria for Standardization of pH Measurements in Organic Solvents and Water + Organic Solvent Mixtures of Moderate to High Permittivities. *Pure Appl. Chem.* **1985**, *57*, 865−876.
(47) Rondinini, S.; Longhi, P.; Mussini, P.; Mussini, T. Autoprotolysis Constants in Nonaqueous Solvents and Aqueous Organic Solvent Mixtures. *Pure Appl. Chem.* **1987**, *59*, 1693−1702.
(48) Barbosa, J.; Sanz-Nebot, V. Autoprotolysis Constants and Standardization of the Glass Electrode in Acetonitrile-Water Mixtures. Effect of Solvent Composition. *Anal. Chim. Acta* **1991**, *244*, 183−191.
(49) Roses, M.; Rafols, C.; Bosch, E. Autoprotolysis in Aqueous Organic Solvent Mixtures. *Anal. Chem.* **1993**, *65*, 2294−2299.
(50) Gagliardi, L. G.; Castells, C. B.; Rafols, C.; Rosés, M.; Bosch, E. Static Dielectric Constants of Acetonitrile/Water Mixtures at Different Temperatures and Debye-Hückel A and a_0B parameters for Activity Coefficients. *J. Chem. Eng. Data* **2007**, *52*, 1103−1107.
(51) Marcus, R. On the Theory of Oxidation-Reduction Reactions Involving Electron Transfer. II. Applications to Data on the Rates of Isotopic Exchange Reactions. *J. Chem. Phys.* **1957**, *26*, 867−871.
(52) Marcus, R. Chemical and Electrochemical Electron-transfer Theory. *Annu. Rev. Phys. Chem.* **1964**, *15*, 155−196.
(53) Marcus, R. A. On the Theory of Oxidation-Reduction Reactions Involving Electron Transfer. I. *J. Chem. Phys.* **1956**, *24*, 966−978.
(54) Miller, J.; Calcaterra, L.; Closs, G. Intramolecular Long-distance Electron Transfer in Radical Anions. The Effects of Free Energy and Solvent on the Reaction Rates. *J. Am. Chem. Soc.* **1984**, *106*, 3047−3049.
(55) Marcus, R. A. Electron Transfer Reactions in Chemistry. Theory and Experiment. *Rev. Mod. Phys.* **1993**, *65*, 599−610.
(56) Johnston, H. S. Large Tunnelling Corrections in Chemical Reaction Rates. *Adv. Chem. Phys.* **1960**, 131−170.
(57) Johnston, H. S.; Parr, C. Activation Energies from Bond Energies. I. Hydrogen Transfer Reactions. *J. Am. Chem. Soc.* **1963**, *85*, 2544−2551.
(58) Cohen, A. O.; Marcus, R. A. Slope of Free Energy Plots in Chemical Kinetics. *J. Phys. Chem.* **1968**, *72*, 4249−4256.
(59) Chandra, A.; Rao, V. S. An Examination of the BEBO Model with the Results of ab initio Calculations of a Reaction Series. *Chem. Phys.* **1994**, *187*, 297−303.
(60) Marcus, R. A. Theoretical Relations Among Rate Constants, Barriers, and Brønsted Slopes of Chemical Reactions. *J. Phys. Chem.* **1968**, *72*, 891−899.
(61) Prémont-Schwarz, M.; Barak, T.; Pines, D.; Nibbering, E. T.; Pines, E. Ultrafast Excited-State Proton-Transfer Reaction of 1-Naphthol-3, 6-Disulfonate and Several 5-Substituted 1-Naphthol Derivatives. *J. Phys. Chem. B* **2013**, *117*, 4594−4603.
(62) Ando, K.; Hynes, J. T. Molecular Mechanism of HCl Acid Ionization in Water: Ab initio Potential Energy Surfaces and Monte Carlo Simulations. *J. Phys. Chem. B* **1997**, *101*, 10464−10478.
(63) Pines, D.; Pines, E. *Solvent Assisted Photoacidity*; Wiley-VCH: Weinheim, Germany, 2007.
(64) Gennett, T.; Milner, D. F.; Weaver, M. J. Role of Solvent Reorganization Dynamics in Electron-transfer Processes. Theory-experiment Comparisons for Electrochemical and Homogeneous Electron Exchange Involving Metallocene Redox Couples. *J. Phys. Chem.* **1985**, *89*, 2787−2794.
(65) Barthel, J.; Buchner, R. High Frequency Permittivity and Its Use in the Investigation of Solution Properties. *Pure Appl. Chem.* **1991**, *63*, 1473−1482.
(66) Vladimirov, E.; Ivanova, A.; Rösch, N. Effect of Solvent Polarization on the Reorganization Energy of Electron Transfer from Molecular Dynamics Simulations. *J. Chem. Phys.* **2008**, *129*, 194515−194515.
(67) Caldin, E. F. Tunneling in Proton-transfer Reactions in Solution. *Chem. Rev.* **1969**, *69*, 135−156.
(68) Headrick, J. M.; Diken, E. G.; Walters, R. S.; Hammer, N. I.; Christie, R. A.; Cui, J.; Myshakin, E. M.; Duncan, M. A.; Johnson, M. A.; Jordan, K. D. Spectral Signatures of Hydrated Proton Vibrations in Water Clusters. *Science* **2005**, *308*, 1765−1769.
(69) Bankura, A.; Chandra, A. Hydroxide Ion Can Move Faster Than an Excess Proton through One-Dimensional Water Chains in Hydrophobic Narrow Pores. *J. Phys. Chem. B* **2012**, *116*, 9744−9757.
(70) Fernandez, M. A.; de Rossi, R. H. On the Mechanism of Ester Hydrolysis: Trifluoroacetate Derivatives. *J. Org. Chem.* **1999**, *64*, 6000−6004.
(71) DeTar, D. F. Tetrahedral Tntermediate in Acyl Transfer Reactions. A Revaluation of the Significance of Rate Data Used in Deriving Fundamental Linear Free Energy Relationships. *J. Am. Chem. Soc.* **1982**, *104*, 7205−7212.
(72) Guthrie, J. P. Hydration of Carboxylic Acids and Esters. Evaluation of the Free Energy Change for Addition of Water to Acetic and Formic Acids and Their Methyl Esters. *J. Am. Chem. Soc.* **1973**, *95*, 6999−7003.
(73) Hedstrom, L. Serine Protease Mechanism and Specificity. *Chem. Rev.* **2002**, *102*, 4501−4524.
(74) Wulff, G. n.; Liu, J. Design of Biomimetic Catalysts by Molecular Imprinting in Synthetic Polymers: the Role of Transition State Stabilization. *Acc. Chem. Res.* **2011**, *45*, 239−247.
(75) Drag, M.; Salvesen, G. S. Emerging Principles in Protease-based Drug Discovery. *Nat. Rev. Drug Discovery* **2010**, *9*, 690−701.
(76) Wilmouth, R. C.; Edman, K.; Neutze, R.; Wright, P. A.; Clifton, I. J.; Schneider, T. R.; Schofield, C. J.; Hajdu, J. X-ray Snapshots of Serine Protease Catalysis Reveal a Tetrahedral Intermediate. *Nat. Struct. Mol. Biol.* **2001**, *8*, 689−694.
(77) Gamcsik, M. P.; Malthouse, J. P. G.; Primrose, W. U.; Mackenzie, N. E.; Boyd, A. S.; Russell, R. A.; Scott, A. I. Structure and Stereochemistry of Tetrahedral Inhibitor Complexes of Papain by Direct NMR Observation. *J. Am. Chem. Soc.* **1983**, *105*, 6324−6325.
(78) Albery, W. J. The Application of the Marcus Relation to Reactions in Solution. *Annu. Rev. Phys. Chem.* **1980**, *31*, 227−263.